Light Metals 2014
Edited by: John Grandfield
TMS (The Minerals, Metals & Materials Society), 2014

CARTOGRAPHY AND CHEMICAL COMPOSITION OF THE DIFFERENT DEPOSITS IN THE HALL-HEROULT PROCESS

François Allard[1], Marc-André Coulombe[1], Gervais Soucy[1], Loig Rivoaland[2]
[1]Université de Sherbrooke; 2500 Boulevard de l'Université, Sherbrooke, Qc, Canada, J1K 2R1
[2]Rio Tinto Alcan (Arvida Research and Development Centre); 1955 Boulevard Mellon, Jonquière, Qc, Canada, G7S 4K8

Keywords: Aluminum electrolysis, Ledge toe, Sludge, Bottom freeze, Alumina, Cathode wear

Abstract

The formation of solid deposits on the cathode surface is problematic for the performance of the electrolysis cell (cathode voltage drop, cell stability, cell life). Furthermore, its mechanism is still not well understood. Although alumina feeding is tightly controlled in industrial cells, the formation of solid deposits is still observed at the interface between the cathode block and aluminum. In order to understand the formation mechanisms and reduce the occurrence of solid deposits, many samples taken from different positions of the interface were analyzed for both the industrial and laboratory electrolysis cells. The effect of the alumina feeding rate and the impact of a thermal gradient on the composition of the deposits were also evaluated. The analysis of industrial and experimental samples demonstrated a concentration gradient of Al_2O_3 and AlF_3 within the deposits implying a variation in the liquidus temperature of the deposit. This study provides insight into the mechanisms responsible for the formation of solid deposits at the cathode surface.

Introduction

In order to maximize the energy efficiency, the electrolysis cells must be operated continuously at lower voltage. By decreasing the energy input, the cell operation is also changed which inversely affects the life of the cell. For instance, the bath superheat temperature becomes lower, the side ledges become thicker and there is more risk of bottom freeze formation on the cathode surface [1]. The deposits at the bottom of the cell can be thicker with higher electrical resistance. Furthermore, the solid deposits located at the bottom significantly reduce the contact surface between the carbon and the aluminum. The formation of solid or solid-liquid deposits in the industrial cell is caused by the two following main phenomena:

- Alumina dissolution and precipitation
- Heat loss at the cathode surface

The dissolution mechanisms of the alumina in the electrolytic bath were studied by several teams in recent decades [2, 3, 4, 5, 6, 7]. The γ alumina phase can dissolve faster than the stable α phase. The dissolution process takes place in two steps, the rapid dissolution of the γ-Al_2O_3 and the slow dissolution process of the α-Al_2O_3. Thus, a feed with higher concentration of α-Al_2O_3 has a higher chance to sink into the bath and to reach the bottom of the cell than a feed containing low concentration of α-Al_2O_3. Moreover, the bath freezes around the alumina particles during the dissolution process due to the endothermic reactions involved in the process as well as the colder alumina feed compared to the liquidus temperature of the bath [7]. If the local density of the agglomerates containing the mixture of bath and alumina exceed the surface tension of the aluminum, these agglomerates can accumulate at the bottom of the electrolysis cell by passing through the aluminum [8]. Moreover, during the anode change, the anode cover material can also fall into the bath. This material with highly concentrated alumina can form deposits on the cathode surface. There are various types of deposits in industrial cells. Figure 1 depicts the main types of deposits.

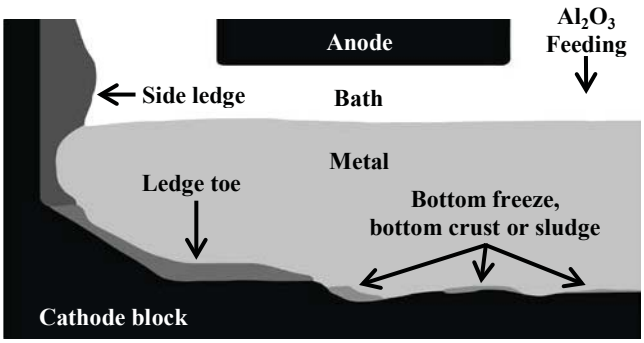

Figure 1. Diagram of the deposits in the electrolysis cell.

The deposits can be either in solid or solid-liquid state at the operating condition. Some solid-liquid deposits such as the side ledge, the ledge toe, the bottom freeze and the bottom crust behave like solids due to their high solid fraction. The previous studies of the sludge showed a mass fraction of 20 % to 50 % alumina, an AlF_3 concentration lower than the bath and a CaF_2 content of about 3 % [8, 9]. During the operation of the electrolysis cell, the sludge consists of the mixture of solid alumina and liquid electrolytic bath saturated in alumina. The deposits highly saturated in alumina like bottom crusts can even reach a mass concentration of alumina in the order of 65 % to 85 % [10]. The bottom crust samples contained a lot of large crystal of α-Al_2O_3 and the crystal can possess a diameter up to the several millimeters.

Methodology

To investigate the formation of deposits in the electrolysis cells, many samples were taken from an industrial cell and from three laboratory cells.

Electrolysis Conditions and Parameters

A laboratory setup has been used to study the deposits formation at the cathode surface. The electrolysis experiments took place under nitrogen atmosphere and the current density was set to 0.7 A/cm^2 (calculated using the cathode block surface). The distance between the anode and the cathode was set to 2 cm. Approximately 400 g of aluminum and 2200 g of the industrial bath with a mass composition of 74 % Na_3AlF_6, 5 % CaF_2, 11 % AlF_3, 9 % α-Al_2O_3 and 1 % γ-Al_2O_3 (cryolite ratio of 2.2) was put in a rectangular carbon cathode block. The cathode block was made of graphitized material. A stream of cold nitrogen gas was

used to drop the temperature of one side of the carbon cathode. The electrolysis cell was placed inside a crucible made of Inconel and installed in an oven to control the electrolysis temperature. Figure 2 shows a top view of the experimental electrolysis cell:

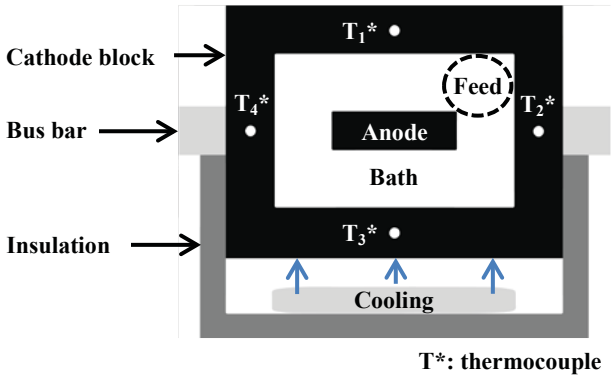

Figure 2. Top view of the experimental electrolysis cell.

The external walls of the experimental cell and the insulation were exposed to the heat flux from the oven. The electrolysis temperature was monitored using the thermocouple T_1. The feeding of alumina was done by a K-Tron powder feeder with a feeding pulse of about 10 to 20 seconds for every two to three minutes. Smelting grade alumina was used in these experiments. Table 1 summarises the parameters of each electrolysis test:

Table 1. Parameters of the Laboratory Electrolysis Tests

Test	Al_2O_3 feeding rate*		Electrolysis time
1	150 % for 1 h	0 % for 3 h	4 h
2	0 % for 2 h	100 % for 4 h	6 h
3	0 % for 2 h	150 % for 4 h	6 h

*Assuming a 60 % electrolysis efficiency

Characterization of Samples

The samples from the industrial cell were taken at various locations on the cathode block surface. The laboratory electrolysis cells have been cut in the horizontal and vertical directions in order to analyze the concentration gradients. To proceed to the analysis, each sample was ground to fine powder using a ball mill.

X-Ray Diffraction (XRD). The powdered samples were placed in a rotating sample holder at a rotation speed of 1 s^{-1} and analysed using a PANalytical X'Pert PRO MPD diffractometer with the Cu Kα ray (wavelength: 0.15406 nm). The total calcium was determined with a XRF Potflux Channel. The data from the XRD was gathered using a PIXcel^{1D} detector equipped with a nickel filter (0.0200 mm). The diffraction pattern was collected at a 2θ from 10° to 74° with a resolution of 0.0263° and a time of 0.12 s per step.

Oxygen Measurement. The powdered samples were placed in a nickel capsule in order to be analyzed. The total oxygen content was determined using a TCH-600 made by LECO.

Scanning Electron Microscopy (SEM). The scanning electron microscope Hitachi S-4700 was used for the purpose of the surface analysis. An acceleration voltage of 20 kV, an intensity of the beam of 10 µA and a working distance of 12 mm were selected. An Oxford X-Max 50 mm^2 Energy-dispersive X-ray spectroscopy module (EDS) was used for elemental analysis.

Optical Microscopy. The optical images were taken by a stereomicroscope Leica of the model MZ FLIII and a numeric camera Leica DC300. The maximum resolution is 3.15 megapixels and the aspect ratio is 4:3.

Quantification of Chemical Species

The results of the XRD analysis were treated by the Rietveld method to quantify the crystalline phases. The composition of the various samples discussed in this article comes from the crystalline phases quantified by Rietveld. The amorphous content of each sample was obtained by adding 20 % of quartz (99.5 % SiO_2) to the sample. The quartz doped samples were re-analyzed by XRD and quantified by the Rietveld method. The following equation is used to calculate the mass fraction of the amorphous content in a sample:

$$w_{amorphous} = \frac{1}{1 - w_1} - \frac{w_1}{w_2(1 - w_1)} \quad (1)$$

Where $w_{amorphous}$ is the mass fraction of the amorphous content in the sample, w_1 is the mass fraction of the quartz added and w_2 is the mass fraction of quartz determined by the Rietveld method. The amorphous quantification gives a very high relative error for the samples with low amorphous content. The error also decreases with increasing concentration of amorphous content [11]. In the result section, the amorphous content is hence given only as an indication. The amorphous content calculated is not distributed on each crystalline phase because the amorphous fraction of each phase is unknown.

The alumina content in the sample was determined by measuring the oxygen balance. A part of the amorphous content is assigned to alumina assuming that all the oxygen detected comes from alumina. The others chemicals compounds that may contain oxygen are neglected. The Rietveld analysis results are only expressed in the form of Na_3AlF_6, CaF_2, AlF_3 and Al_2O_3 species in order to simplify the presentation. Thus the molecules of $Na_5Al_3F_{14}$, $NaAlF_4$, $NaCaAlF_6$, $Na_4Ca_4Al_7F_{33}$ and $NaCa_{1.5}AlF_7$ species have been simplified by elemental balance.

Thermodynamic Equilibrium Calculations

The phase diagrams in the equilibrium condition were calculated using the FactSage software (version 6.4). The software calculates the chemical species concentration by minimising the Gibbs free energy. The thermodynamic equilibrium calculation was carried out using the XRD data about the chemical composition of the samples as well as the alumina content obtained by the oxygen determination.

Results

To understand the mechanisms of deposits formation, many samples have been collected at different locations of an industrial electrolysis cell. These samples were then compared with the samples collected from the laboratory cells.

Industrial Samples

The industrial samples come from a stopped cell after 1200 days of operation where the cathode block was heavily covered by thick deposits. These thick deposits were mainly located at the position of the ledge toe (positions B, C and D in Figure 3) next to the area with excessive erosion of the cathode block. Few thick deposits were observed between the ends of the ledge toe and the center of the industrial cell. The deposits become thinner toward the center of the cell (their thickness was in the order of a few millimeters). These thin deposits were distributed like spots on the cathode surface. Only thin deposits were observed under the feeder position (position A in Figure 3). The average chemical composition of the four samples taken from the position A is presented in the first line of Table 2. The crystalline part of these thin deposits contained only α-Al_2O_3. None of the transition form of alumina (γ-Al_2O_3, β-Al_2O_3, δ-Al_2O_3 or θ-Al_2O_3) was observed. The samples of the side ledge and the ledge toe have been collected based on their position and their height from the cathode in order to determine the concentration gradient. The next diagram shows the location where the deposits were taken:

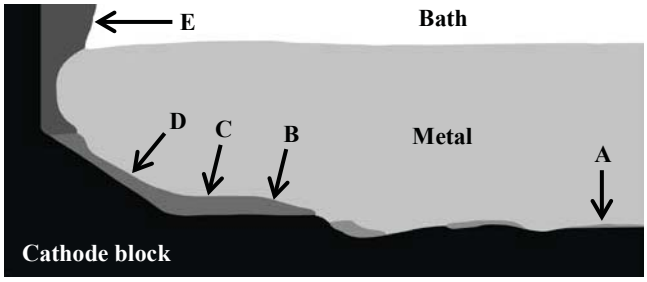

Figure 3. Positions of the deposits taken in the electrolysis cell.

The Table 2 shows the chemical composition of the sample A to E. T_{liq}, T_{trans} and the amount of solid alumina at 960 °C have been predicted using FactSage software based on the composition of the samples measured by XRD. The transition temperature, T_{trans}, corresponds either to the transition of the cryolite solution when the sample is supersaturated in alumina or to the transition of the alumina when the sample is under saturated. The height column indicates the distance measured from the cathode surface to the top of the sample. A mass concentration gradient of Al_2O_3, AlF_3 and CaF_2 were observed inside the sample at the extremity of the ledge toe (sample B). However, the fraction of electrolytic bath in the sample is highly diminished as a result of higher amount of solid alumina. To neglect the impact of the alumina concentration in the analysis of the deposit chemistry, the cryolite ratio and the equivalent concentration of CaF_2 has been used. This hypothesis is made in order to better understand the behavior of the electrolytic bath in the sample with the solid alumina. Furthermore, the electrolytic bath fraction of the sample is saturated in alumina at operating condition. The equivalent mass concentration of CaF_2 is calculated as follow:

$$w_{CaF2eq} = \frac{w_{CaF2}}{1 - w_{Al2O3}} \quad (2)$$

Where w_{CaF2} is the mass fraction obtained by Rietveld quantification and w_{Al2O3} is the mass fraction obtained by alumina balance of the oxygen determination.

It is not possible to make a conclusion for each of industrial samples at a specific position according to their variation in the cryolite ratio or CaF_2 concentration, as shown in the Table 2. However, there are important differences in the cryolite ratio between the samples depending on the position in the electrolysis cell. This observation is discussed further. The amorphous content of the sample is given as an indication and it is the part of the electrolytic bath which could not be quantified. The total content in alumina was quantified by elemental oxygen analysis. The difference between the crystalline alumina measured by XRD and the result of the elemental oxygen analysis has been considered as the amorphous content. The alumina quantification is useful to distinguish the under saturated samples from the supersaturated samples. For instance, the sludge is a supersaturated deposit and it contains solid alumina suspended into the liquid bath. These calculated transition temperatures are reported in the Table 2.

Table 2. Mass Concentration of the Thin Deposits, the Side Ledge and the Ledge Toe

Sample	Height (mm)	Na_3AlF_6 (%)*	CaF_2 (%)*	AlF_3 (%)*	Al_2O_3 (%)*	Amorphous (%)**	Cryolite Ratio	CaF_{2eq} (%)	T_{liq} (°C)	T_{trans} (°C)	$Al_2O_{3(s)}$ at 960 °C (%)
A	-	64 ± 9	5 ± 0.4	5 ± 0.6	26 ± 9	13 ± 9	2.5	7	1395	942	20
B	24-32	44	3	4	49	12 ± 4	2.5	6	1753	944	45
	16-24	36	2	4	58	12 ± 4	2.4	5	1825	942	55
	8-16	34	2	3	61	6 ± 5	2.5	5	1844	943	57
	0-8	28	2	2	68	15 ± 2	2.5	5	1895	948	65
C	20-30	77	6	13	4	28 ± 4	2.1	6	941	906	-
	10-20	78	6	14	2	39 ± 3	2.0	6	948	880	-
	0-10	80	6	12	2	39 ± 3	2.2	6	959	886	-
D	14-24	81	5	12	2	26 ± 4	2.2	5	960	888	-
	0-14	81	5	12	2	24 ± 4	2.2	5	962	859	-
E	-	80 ± 1.0	6 ± 0.5	12 ± 0.4	2 ± 0.5	28 ± 4	2.2	6	957	890	-

*In this column the symbol ± is the standard deviation; **in this column the symbol ± is the measurement error.

Industrial Samples with Supersaturated Al_2O_3. The sample at the extremity of the ledge toe (sample B in Table 2) is highly concentrated by α-Al_2O_3. There is a concentration gradient of alumina in this sample. The bottom part of the sample, nearer to the cathode surface, is more concentrated in alumina than the top resulting in more solid alumina than liquid bath at operating temperature. In fact, 65 % of the sample was determined to be in solid state at 960 °C according to the thermodynamic analysis.

The liquidus temperature of the sample B is very high which can be attributed to the significant content of α-Al_2O_3 is. Thus the dissolution process of this sample in the bath is slow. Many alumina crystals with some millimeters of width have been observed by optical microscope and by SEM-EDS. The Figure 4 shows some alumina crystals in the sample B which is located at the ledge toe extremity:

Figure 4. Alumina crystals observed by optical microscope.

The same area has been observed by SEM (Figure 5) and the oxygen has been detected by EDS. The black spots represent the area concentred in oxygen:

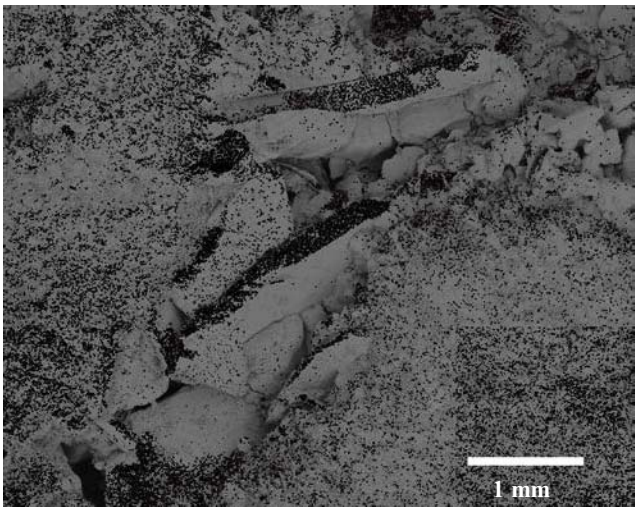

Figure 5. Alumina crystals observed by SEM-EDS.

These crystals can also be seen with the naked eye and they have slightly bright reflections. The color of the crystals is either brown or golden. The crystals have been seen mainly in highly alumina concentrated areas. They can grow during the solidification of the bath which is supersaturated in alumina. According to their shape and dimension, the dissolution rate will be slower compared to the feeding alumina. The sample C, D and E are under saturated in alumina and they can only be solid if the local temperature is low enough (under the transition temperature of the cryolite solution).

Cryolite Ratio of Industrial Samples. The cryolite ratio as a function of the position remained relatively uniform for the industrial samples. Nevertheless, the surface deposits (sample A) and the deposits at the extremity of the ledge toe were more neutral than the side ledge and the base of the ledge toe. The deposits with supersaturated alumina were more neutral than the under saturated alumina which are more acidic.

Laboratory Samples

The laboratory samples come from the experimental tests with the setup shown in the Figure 2. The deposits were collected by cutting the experimental cell into slices and by retrieving the samples around the aluminum. The results of the test 2, with an alumina feeding rate close to the stoichiometric value, are shown in the Figures 6 and 7. The left wall is far from the feeder in contrast of the right wall. Figure 6 shows the cryolite ratio at both sides:

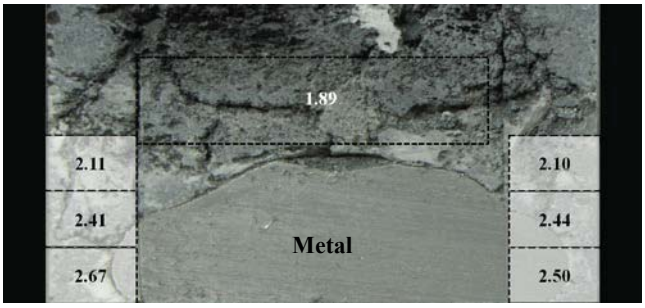

Figure 6. Cryolite ratio of the samples from test 2.

There was a vertical gradient related to the cryolite ratio. The samples were more neutral closer to the cathode surface. The cryolite ratio gradient can be explained by the migration of the sodium ions to the cathode [12]. There was also an acidification of the bath above the metal during the experiment (the cryolite ratio at the beginning was 2.2). As in industrial cells, the observations revealed the presence of a very thin deposit under the aluminum. Figure 7 shows the alumina gradient in the same test:

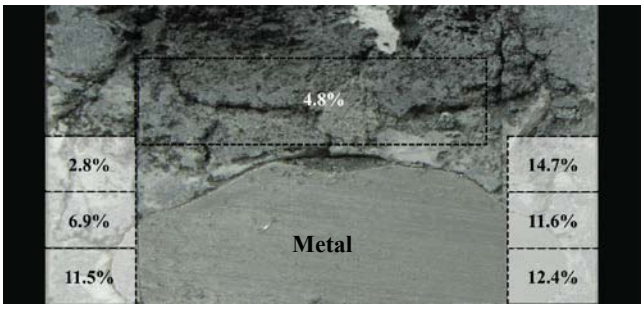

Figure 7. Al_2O_3 mass fraction of the samples from test 2.

Far from the feeding area, there was an important alumina vertical gradient. In the same location, the top and middle samples were under saturated in alumina while the sample at the bottom was slightly supersaturated in alumina. The saturation of the sample was calculated by thermodynamic equilibrium at the operation temperature. The samples close to the feeding position were even more supersaturated due to the sinking of the alumina particles to the bottom of the cell. However, the density is not high enough to create an accumulation under the metal. The magnetohydrodynamic movement in the metal is also very slow compared to the movement in an industrial cell. In the industrial cells, the alumina is added above the middle of the metal. The Figures 8 and 9 show the results of the alumina overfeeding experiment (test 3):

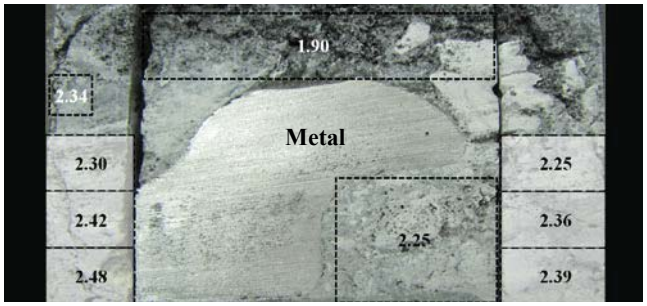

Figure 8. Cryolite ratio of the samples from test 3.

The electrolytic bath above the metal was acidified during the electrolysis test. There was again a vertical gradient of acidity in the samples taken around the metal. A white sample located at the left side of the Figure 9 has been collected on the carbon wall far from the feeding. This sample containing lower alumina (1.1 %) was more neutral than the bath. During the operation, this sample was colder than its liquidus temperature (967 °C). The aluminum has been raised by the bath supersaturated in alumina. The acidity of this sludge was similar to the starting bath (cryolite ratio of 2.2). Figure 9 shows the mass concentration of alumina:

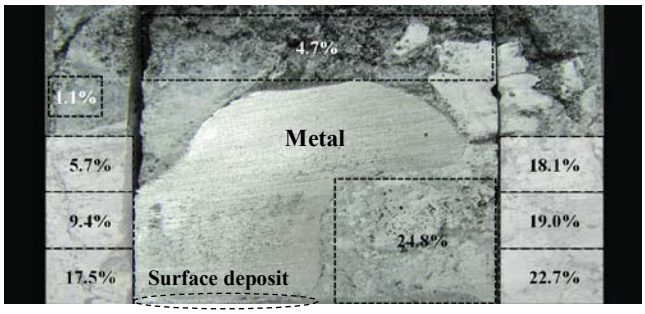

Figure 9. Al_2O_3 mass concentration of the samples from test 3.

The sludge has lifted the aluminum up because the density of this mixture is higher than the density of the aluminum. The sludge contains 6.1 % of Al_2O_3 dissolved in the bath fraction and 18.7 % of $Al_2O_{3(s)}$ at 960 °C according to thermodynamic analysis. The calculation of the density is discussed further. A surface deposit has been observed between the metal and the carbon block. It contained 21 % Al_2O_3 and the cryolite ratio was 2.34.

Close to the cooled wall of the test 3, a ledge toe deposit has been observed and the aluminum followed the shape of the deposit (Figure 10).

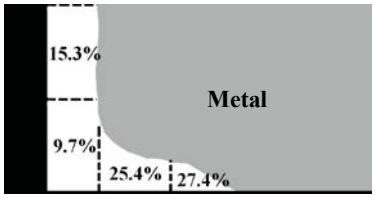

Figure 10. Al_2O_3 mass fraction of the samples near of the cooled wall.

The cold wall was cooled to a temperature of 925 °C. The cryolite ratio of the sample close and away from the cold wall was 2.45 and 2.28, respectively. The calculated density of the ledge toe was higher than the aluminum.

The test 1 was used to verify the impact of the both overfeeding and anode effect on the alumina concentration in the bath. The alumina concentration in the bath decreased to approximately 3 %. Despite the fact that anode effect was reached after 4 hours of electrolysis, the mass concentration of the alumina at the bottom of the cell remained at an average of 12 %. Thus, there was a poor vertical distribution of the alumina in the experimental cell. The metal acted as a barrier for the diffusion of the alumina in the bath underneath of the metal.

Thermodynamic Results

A thermodynamic study has been done in order to better understand the behavior of the deposits depending on the concentration of alumina and the cryolite ratio. The next figure shows a phase diagram which represents the composition of the deposit:

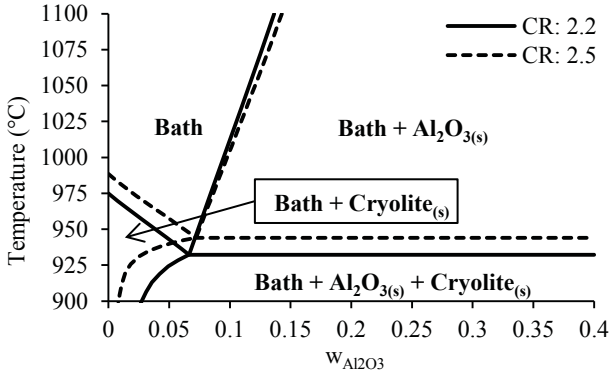

Figure 11. Phase diagram of the bath as a function of alumina mass fraction.

The calculation has been done using cryolite ratios of 2.2 and 2.5 with a constant mass concentration of CaF_{2eq} of 5 %. The transition temperature of the cryolite solution decreases when the acidity increases. The deposits that are more neutral present more risk to reach the temperature of transition of the cryolite solution. The liquidus temperature is strongly influenced by the concentration of Al_2O_3 in the sample. The solidus temperatures are 696 °C with a CR of 2.2, 705 °C with a CR of 2.5 and 917 °C with a CR of 2.8. The solidification interval takes place in a wide range of temperature. This wide temperature interval can be partially explained by the augmentation of the AlF_3 concentration in the liquid bath as the solid part is formed. Thus, the local composition of the liquid can change during the precipitation of the other solid phases.

Discussion

Alumina Overfeeding. The formation of solid deposit or solid-liquid deposit can be explained in many ways. The denser alumina particles will sink toward the cathode surface when their weights exceed the surface tension of the aluminum. The alumina can also sink between the metal and the side wall as shown in the experimental tests. The density of the saturated bath, or the mixture of bath and solid alumina, is very important for understanding if a part of the bath will sink toward the bottom of the electrolytic cell. During the feeding by batch of the alumina, a formation of solid bath around the alumina particles occurs. Therefore, this aggregate can sink into the bath. The under saturated bath will not sink toward the bottom of the cell because its density decreases with increasing alumina content in solution [13]. Once saturation is reached, the density will begin to increase. The sludge sample in test 3 lifted the aluminum pad. This sample contained 24.8 % of Al_2O_3 and had a CR of 2.25. The aluminum density at 960 °C is 2.30 g/cm^3, the density of the saturated bath is 2.06 g/cm^3 and the density of alumina particles in bath is 3.89 g/cm^3 [13, 8]. Once the sludge reaches a mass concentration higher than 20 % of alumina, its density exceeds the metal's density at a temperature of 960 °C.

Effect of Temperature. The local temperature is used to calculate the solid-liquid fraction of the deposits supersaturated in alumina. The supersaturated deposits behave like sludge when their temperature is below their liquidus temperature and above the transition temperature of the cryolite solution. If the deposit is greatly supersaturated (bottom crust), it can behave as a solid crust. When the local temperature of a supersaturated deposit is below the transition temperature of the cryolite solution, the deposit will be harder to dissolve.

Impact of Aluminum and MHD. The aluminum acts as a physical separation between the deposits and the electrolytic bath. In the industrial cells, the magnetohydrodynamic movements in the metal make possible the backfeeding of the alumina from the soft sludge [14]. The centrifugal effect of the metal movement distributes the alumina particles around the cell and the ledge toe will be in contact with alumina. The bath film between the side ledge and the metal can dissolve the supersaturated deposits at the bottom of the cell. The aluminum pad has a high density and it applies a force on the bath and on the slightly supersaturated deposits making them to move toward the periphery of the electrolytic cell.

Equilibrium Between Sludge and Ledge Toe Deposits. The supersaturated deposits at the bottom of the cell exchange alumina. However, the ledge toe has a greater solid fraction than the sludge as a result of the heat loss caused by the sidewall. The slightly supersaturated sludge is more mobile and it can be displaced by the metal weight. The sedimentation of alumina in the bath increased the alumina concentration in the deposits.

Conclusion

The study of the various industrial and laboratory deposits provides clarification about their compositions and mechanisms of formation. The laboratory cells can reproduce the operating conditions of industrial cells in order to understand the behavior of the deposits. With this knowledge, the operating conditions of electrolysis cells can be adjusted in order to reduce the operating costs. The density and the local temperature are the important parameters to be monitored. Depending on the density, a supersaturated deposit can lift the metal.

Future Work

The future work should aim the impact of cryolite ratio on the deposits formation. The thermodynamic study will be developed for the purpose of understanding the phase transitions in the various deposits. The solid-liquid fraction of the deposits will be studied to evaluate their behavior during the operation.

Acknowledgements

The authors are grateful to the employees of the "Centre de Caractérisation des Matériaux" for their help with the various characterization devices, especially Carl St-Louis, Irène Kelsey-Lévesque and Sonia Blais. Thanks for the mechanical engineering technician, André Bilodeau, who help on the experiment. The work has been made possible with the financial support of Rio Tinto Alcan, "Conseil de Recherches en Sciences Naturelles et en Génie du Canada" (CRSNG) and "Fonds Québécois de la Recherche sur la Nature et les Technologies" (FQRNT).

References

1. H. Kvande and W. Haupin, "Cell Voltage in Aluminum Electrolysis: a Practical Approach," *JOM*, 52 (2) (2000), 31-37.
2. X. Wang, "Alumina Dissolution in Aluminum Smelting Electrolyte," *Light Metals*, 2009, 383-388.
3. B. J. Welch and G. I. Kuschel, "Crust and Alumina Powder Dissolution in Aluminum Smelting Electrolytes," *JOM*, 59 (5) (2007), 50-54.
4. R. G. Haverkamp and B. J. Welch, "Modelling the Dissolution of Alumina Powder in Cryolite," *Chemical Engineering and Processing: Process Intensification*, 37 (2) (1998), 177-187.
5. K. Tørklep, K. Kalgraf and T. Nordbø, "Alumina Distribution in Point-Fed Hall-Héroult Cells," *Light Metals*, *1997*, 377-386.
6. B. Lillebuen, T. Mellerud and K. Thovsen, "Alumina Dissolution in Point-Fed Cells," *Light Metals*, 1992, 449-452.
7. S. Rolseth, R. Hovland, and O. Kobbeltvedt, "Alumina Agglomeration and Dissolution in Cryolitic Melts," *Light Metals*, 1994, 351-357.
8. R. Keller, "Alumina Dissolution and Sludge Formation Revisited," *Light Metals*, 2005, 147-150.
9. P. Y. Geay, B. J. Welch and P. Homsi, "Sludge in Operating Aluminium Smelting Cells," *Light Metals*, 2001, 541-547.
10. J. Thonstad, S. Ronning and P. Entner, "Formation of Bottom Crusts in Aluminum Pots - a Laboratory Study," *Light Metals*, 1982, 485-497.
11. T. Westphal T. Füllmann and H. Pöllmann, "Rietveld Quantification of Amorphous Portions with an Internal Standard - Mathematical Consequences of the Experimental Approach," *Powder Diffraction*, 24 (3) (2009), 239-243.
12. P.-Y. Brisson et al., "Revisiting Sodium and Bath Penetration in the Carbon Lining of Aluminum Electrolysis Cell," *Light Metals*, 2005, 727-732.
13. J. Thonstad et al., *Aluminium Electrolysis: Fundamentals of the Hall-Héroult Process* (Düsseldorf, Germany: Aluminium-Verlag, 2001), 96.
14. K. Kalgraf and K. Tørklep, "Sediment Transport and Dissolution in Hall-Héroult Cells," *Light Metals*, 1998, 455-464.